Zeng, Jinming; Lu, Wei; Paavola, Juha

Ultimate strength of a beam-to-column joint in a composite slim floor frame

Published in:
Journal of Constructional Steel Research

DOI:
10.1016/j.jcsr.2017.10.009

Published: 01/01/2018

Document Version
Peer-reviewed accepted author manuscript, also known as Final accepted manuscript or Post-print

Ultimate strength of a Beam-to-Column Joint in a Composite Slim Floor Frame

Jinming Zeng[a], Wei Lu[a], Juha Paavola[a]

[a]Department of Civil Engineering, School of Engineering, Aalto University, P.O.Box 12100, FI-00076 Aalto, Finland

Abstract

The paper studies numerically the behavior of a beam-to-column joint between a hat-shaped steel beam (WQ-beam) and a concrete-filled composite column in a slim floor steel-concrete composite frame. 3D continuum elements are used in the discretization of the joint with contact surfaces between the components. Both material and geometrical nonlinearities are included. The computational results are verified by comparing them to experimental results. The verified model is applied to study the development of the load-transfer mechanisms in the joint. The load carrying capacity of the joint is categorized on the base of five parameters: the flange width, the web height, the wall thickness and the corners of the console, and the gap between the WQ-beam endplate and the column face. In addition, a criterion to evaluate the limit load of the joint is proposed. The design capacity of the joints from the proposed criterion is compared with the values calculated according to both other criteria and design code. It can be concluded that the proposed criterion is suitable for estimating the resistance of the studied joint.

Keyword: Slim-floor system, Beam-to-column joint, Tubular joint, Ultimate strength, Deformation limit, Yield load.

1 Introduction

A slim floor system is constructed by containing the supporting steel beams within the depth of the floor deck. The slim floor systems have been extensively applied in commercial and residential buildings, hospitals etc. because it provides a floor system with minimum constructional depth, and it offers important benefits in terms of cost and fire resistance. The structural behaviour of composite slim floor system has been studied in terms of the integrated composite slim floor beam and in terms of the connection between the asymmetric slim floor steel beams and columns [1-6].

One type of slim floor beam, called WQ-beam, has been manufactured and widely applied in Nordic Counties. The WQ-beam is hat-shaped, torsional-rigid, box beam and is intended to speed up erection of multi-storey buildings due to the use of the standardised steel and precast concrete elements. Several types of joints, such as claw joint, bolt joint, or bracket joint have been used to connect WQ-beam and column [7]. A novel beam-to-column joint for connecting WQ-beam to concrete-filled composite column has been developed in recent years because of low construction costs, simple installation process, high installation tolerance, and easily ensured quality control. The main components of the joint include circular concrete-filled composite column, WQ-beam with an endplate, steel console with an endplate, and tension-bar shown in Fig. 1 (a). The steel console (short RHS tube) is welded to the concrete filled CHS columns in the factory. At construction site, the WQ-beam can be released from the crane after it has been put down to the console. The endplate of the WQ-beam is cross on the top flange of the steel console. The tension-bar, which is inserted through the column, is designed as lateral bracing and will be welded to the column and the WQ-beam at the construction site. The floor slab can be hollow-core or composite concrete slab with a concrete topping.

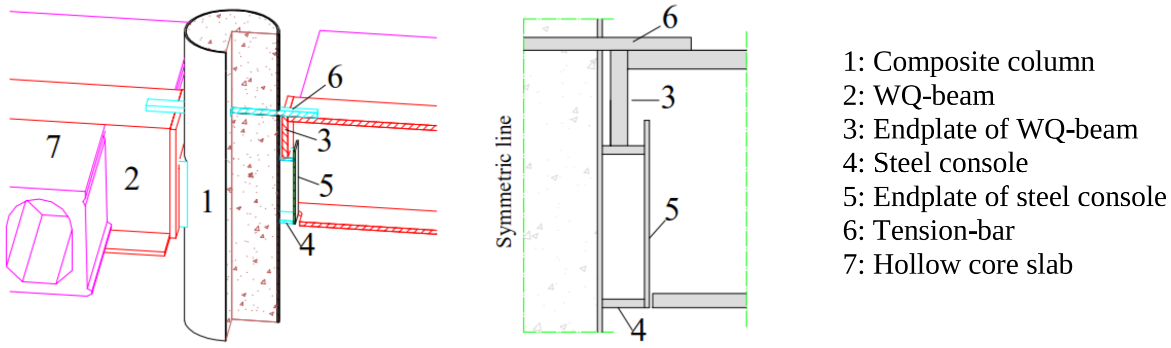

(a) (b)

Fig. 1. A novel joint for composite slim floor frame. (a) Main components of the joint; (b) Detailed components of the joint.

Since design rules, related to this type of joints, are neither provided in EN 1994-1-1 [8] nor in EN1993-1-8 [9], a series of static tests have been performed on full-scale double-sided beam-to-column joints by the research group at Tampere University of Technology [7]. The results of one type of joint have been sent to the authors' research group for further studies. From the test results [7], especially from the load-deformation curves, two phenomena are noticed: no clear value for the yield load can be observed; and the peak loads have normally been reached through large deformations in most tests. For the joint studied in this paper, the peak load has not even been reached before the termination of the tests to protect the testing equipment. It seems that the joints exhibit high ductile behaviour because the loads carried by the joint still increase after initial yielding. Therefore, it is necessary to further investigate the load transferring mechanisms inside the joint; and check if the large deformations in joint are acceptable for determination of the capacity of the joint. Further investigation, on selecting a suitable failure criterion for the limit capacity, is necessary.

In this regard, a 3D finite element model is constructed by using the general purpose finite element software ABAQUS [10]. ABAQUS/Explicit is selected because it can effectively handle severely nonlinear behaviour of structures, for instance contact problems. The FE results are validated by the test results and the load transferring mechanisms inside the joint are investigated. Accordingly, different criteria used to determine the ultimate capacity of the joint are discussed. Finally, five parameters, which presumably have the main influence on the ultimate capacity of the joint, are concluded and eventually, a reasonable criterion is proposed, based on the results of parametric studies. The proposed design strength is evaluated by using the design equations which are provided for general joints.

2 Three-dimensional finite element model

2.1 Geometry of the joint

Totally, nine full-scale double-sided beam-to-column joints were investigated in the tests. One of the joint tests is chosen to be used in verifying the FE model. The FE model is created as based on the test setup as shown in Fig. 2 (a). One end of the WQ-beam is supported by a roller while the other is connected to the column by the joint considered (see Fig. 1). The base of the composite column is bolted rigidly to the laboratory floor. The loading is generated through four identical hydraulic actuators, and it is transmitted to the WQ-beams by drawbars that are connected to loading-beams on top of the WQ-beam. The distance between the drawbars on each side of the beam is 700 mm. The middle line of one side loading-beam is at the distance of 350 mm measured from the centre of the column. No axial load is applied to the column.

Since the joint under consideration is symmetric about composite column, only one half of it is modelled, as shown in Fig. 2 (b), in order to improve the computation efficiency. Table 1 shows the dimensions of each component of the joint specimen. All welds in the joint are fillet welds except the top flange of the console which is fixed to the column by a groove weld. The weld size between the console and the column is 6 mm. An endplate is welded to the other end of the console with weld size of 5 mm, likewise the tension-bar to the hollow steel section and to the WQ-beams.

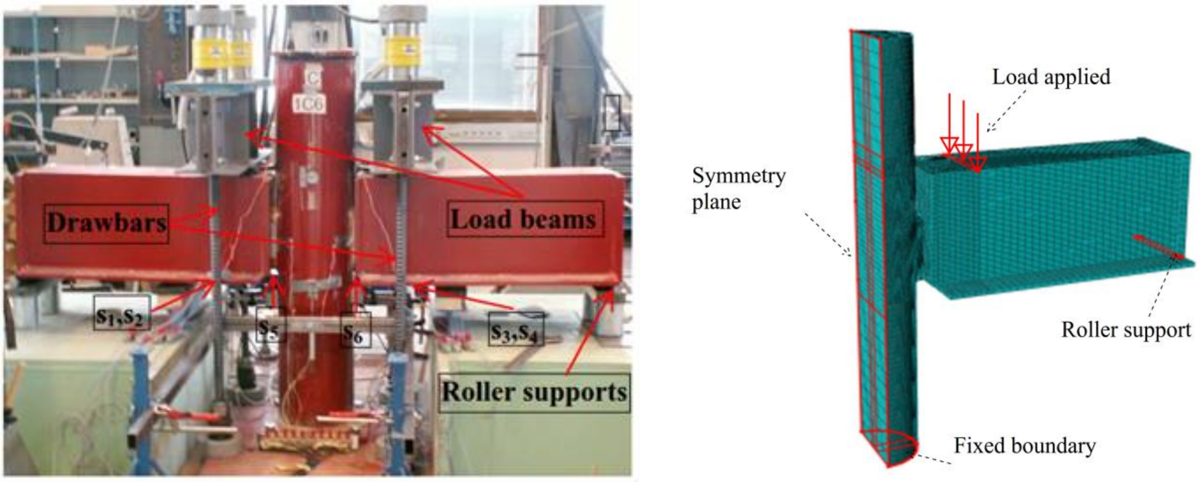

(a) (b)

Fig. 2. Geometry of the joint. (a) Test; (b) FE model.

Table 1. Dimensions of test specimen (mm)

Dimensions		Composite column	WQ-beam			WQ-beam endplate	Steel console	Console endplate	Tension-bar
			Top flange	Webs	Bottom flange				
Cross-section	Width	323,9	290	-	570	330	150	150	50
	Height	-	-	400	-	415	250	280	20
	Thickness	6	20	6	15	20	10	6	-
Height or Length		1530	1000	1000	1000	-	50~64	-	584

2.2 Material properties

The structural steel for WQ-beam, hollow steel column, console and tension bar are modeled as elastic-plastic material with isotropic hardening both in compression and in tension. The von Mises plasticity criterion is used to define the yield surface. The yield strength and ultimate strength are 355 MPa and 510 MPa, respectively. The modulus of elasticity, E_s, and Poisson's ratio,v_s, are assumed to be 210 GPa and 0.3, respectively. The strain of steel at the ultimate strength is defined to be 20%. True stress and true strain as input are required by the analysis software, and hence the engineering stress and strain are converted to true stress and true strain.

The material properties of the concrete in the composite column are simulated by using Damaged Plasticity Model in ABAQUS because it affords a possibility for the analysis of concrete structures under static, dynamic, or cyclic loading. The inelastic behaviour of concrete is defined by combining the isotropic tensile and compressive plasticity. The stress-strain curves of concrete in uniaxial compression and tension are employed in the FE model. The values of the stress and strain are calculated according to EN 1992-1-1 [11]. The grade of the concrete is C35/45. The parameters in this model have constant values; dilation angle ψ is 30°, the flow potential eccentricity e is taken to be 0.1, the compressive meridian K_c is 2/3 and the ratio of the compressive strength under biaxial loading to uniaxial compressive strength f_{b0}/f_c is 1.16. The tension stiffening is assumed to take place when the cracking displacement reaches the value of 1 mm.

2.3 Element types and mesh

The composite column, WQ-beam, WQ-beam endplate, steel console, steel console endplate and tension-bar are modeled using eight-node brick elements with reduced integration (C3D8R) because these elements have the capability to represent geometric and material non-linearity, and they are of sufficient accuracy with reasonably low computational time and thus also costs. The welds are simulated by using tetrahedral elements with hourglass control (C3D10M). They are geometrically versatile and are suitable for automatic meshing algorithms. The longitudinal reinforcing bars inside the composite column are modelled by two-node, first-order truss elements (T3D2). The stirrups are not simulated in the model.

In order to get accurate results, the fine mesh is adopted in the vicinity of joint regions where high stresses and strain gradients are expected to take place. The effect of hourglass can be avoided if at least four elements are used through the thickness of the cross-section. Consequently, six layers of elements along the thickness of cross-section in the console are used, resulting in the mesh size of 1.5 mm. The mesh size of the tension-bar is 4 mm. In addition, the mesh sizes for welds, console endplate, WQ-beam, steel tube of the column, and concrete core of the column inside connection regions are 3 mm, 3 mm, 10 mm, 5 mm, and 10 mm, respectively.

2.4 Boundary conditions and loads

The composite column is fixed at the bottom in order to simulate the column base plates, as shown in Fig. 2(b). Since a roller support is used at the bottom of endplate of the WQ-beam, the endplate of the WQ-beam is allowed to move freely only in the horizontal direction, while the vertical displacement is prevented. On the plane of symmetry, the displacements of all nodes are prevented to move towards the symmetry plane. The deformation-controlled loading, which simulates the static loading in the tests, is applied gradually on the top flange of the WQ-beam. The width of the loaded area is 20 mm and the centre of it is at the distance of 350 mm away from the centre of the column. The FE analyses are set to be interrupted when the displacements ($S1$ – $S4$ as shown in Fig. 3 underneath the WQ-beam along the loading line reach the value of 25 mm.

2.5 Interface between the components

The reinforcements are embedded inside the concrete column. Surface-based tie contact interaction is used to connect welds to the surfaces of the components such as WQ-beam, tension-bar, and column. The contact surfaces of the welds are always set to be master surfaces while the other contact surfaces as slaves. Surface to surface contact interactions are defined between the WQ-beam endplate and the console, as well as between the steel and concrete. In this contact interaction, the friction formulation between the contact surfaces is simulated by using Coulomb friction model (Penalty). “Hard-contact” is chosen to simulate the normal behavior. Finite sliding is selected because this approach allows arbitrary separation, sliding, and rotation of the surfaces.

3 Validation of FE model against experimental test results

The loading applied to the WQ-beam (P_B, P_D) and reactions at the ends of WQ-beam (T_B, T_D), as shown in Fig. 3 (a), are measured in the test. According to the equilibrium conditions of the WQ-beam and of the joint, the forces in the joint (V_B, V_D) and in the column (Q) can be calculated by the following equations:

$$V_B = P_B - T_B \qquad V_D = P_D - T_D \qquad Q = V_B + V_D \tag{1}$$

In the test, the vertical displacements ($S1$ – $S4$) underneath the WQ-beam webs along the loading lines are monitored both on the left-side ($S1$, $S2$) and the right-side of the column ($S3$, $S4$), respectively. The displacements of the console relative to the column shaft are recorded at the bottom of the console both on the left hand ($S5$) and right hand sides ($S6$) of the column, respectively. The front-side displacement ($S7$) and back-side displacement ($S8$) of column shaft with respective to the base-plate are recorded, respectively. The detailed location of the transducers is shown in Fig. 3 (b).

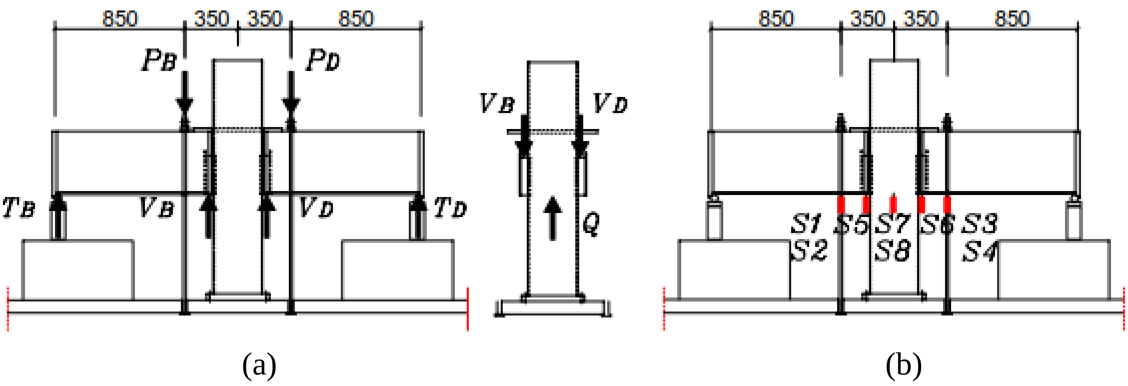

Fig. 3. Location of load and displacement. (a) Locations of loads in joint; (b) Locations of displacements transducer. All measures in mm.

Fig. 4 (a) shows the comparison between load-displacement curves of WQ-beam measured in the test (P_B –average value at $S1$ and $S2$ (left side) and P_D - average value at $S3$ and $S4$ (right side)) and the corresponding ones of numerical analysis. Fig. 4 (b) compares the load versus relative displacement distributions at joint, measured in the test (V_B - $S5$ and V_D - $S6$) with the ones of FE-analysis. In Fig. 4 (c) the comparisons between load-deflection curves for the column shaft (Q – average value of $S7$ and $S8$) are shown similarly. In numerical results, all the observations from experimental tests can be detected. Fig. 4 (d) shows the ratio of the force transferred by the console (V_c) to the force transferred by the joint (V). It can be seen that the load carried by the console accounts for at least 94% of the one carried by the joint.

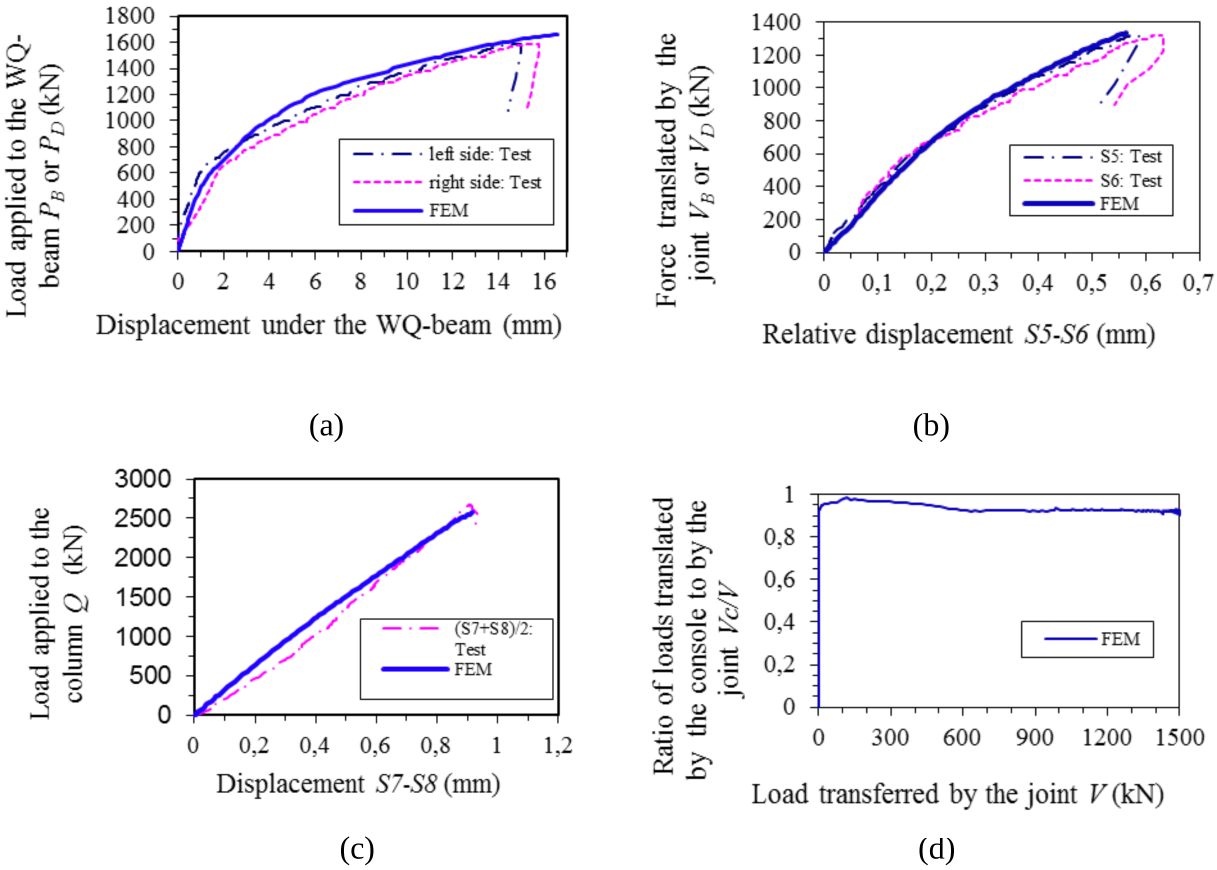

Fig. 4. Comparison between measured and FE results. (a) Load-deflection curves measured under WQ-beam; (b) Load-deflection curves for the joint; (c) Load-deflection curves for column; (d) Ratio of the load carried by the console to the joint.

The deformed shape of the console from FE analysis when the displacement at $S1$ has reached the value of 15.8 mm, is compared to the deformed shape observed in the experimental test as shown in Fig. 5. It can be seen that the deformed shape of the console from FE analysis shows good agreement with those observed in the test. The indentation of the top flange of the console and the curling of the endplate of the console to the column are both observed.

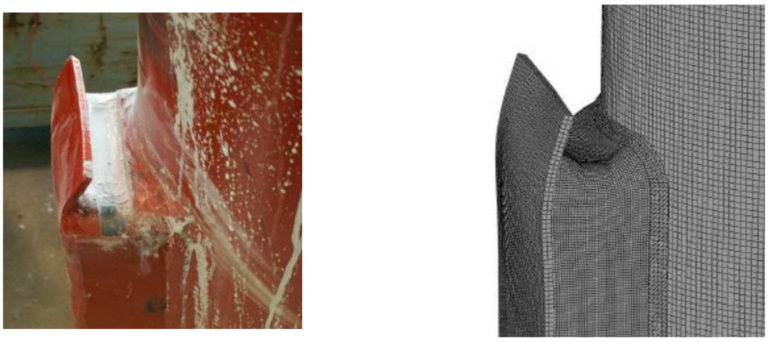

(a) (b)

Fig. 5.Comparison of deformed shapes: (a) Final deformed shape from test; (b) Deformed shape at *S*1 = 15.8 mm from FE analysis.

Considerable indentation at the console has been observed in the final deformation shape as shown in Fig. 5. Therefore, indentation is investigated firstly. The value of indentation can be estimated from the measured values of displacements both on the beam and column using the model shown in Fig. 6 (a). WQ-beam has so high bending stiffness that it can be assumed to rigidly rotate around point a. The value of the displacement at point b can thus be calculated based on the displacement (*S1*-*S4*) at point c. On the other hand, the displacement at point b is the sum of the indentation of console (δ), the relative displacement (*S5* or *S6*), and the displacement (*S7* or *S8*). By equating the displacement at point b, the indentation of console can be estimated. Fig. 6 (b) shows the comparisons of load-indentation curve from test results to that from FE analysis. The indentations from test results are calculated by applying the abovementioned model. The indentations from FE analysis are directly taken from output results. It can be seen that two results show good agreements.

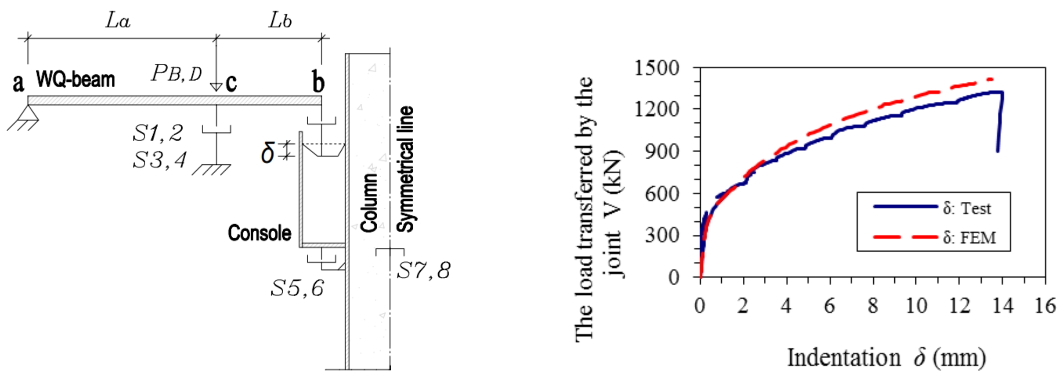

(a) (b)

Fig. 6 Comparisons of load-indentation curves from both test and FE results. (a) Principle of calculation of indentation for test results; (b) Load-indentation curves obtained from both FE analyses and the test.

4 Load transferring mechanism in joint

In general, the load on the console is transferred to the column by means of three mechanisms: the shear of the webs (C), the bending of both webs and flanges (M), and the membrane tension (T) developed in the top flange due to large indentation. These three mechanisms are shown in Fig. 7 (a) to (c), respectively. The behaviour of the joint is influenced by the variations of the load transferring mechanisms mentioned above, which can be reflected through both strain-load and indentation-load curves as shown in Fig. 8 (a) and (b); and through maximum and minimum principal stresses from FE analysis at selected deformations as shown in Fig. 9 (a) to (d), respectively.

The load is mainly transferred by web shear and cross-section bending until 509 kN. From Fig. 8 (a), it can be seen that the tension strain of L63 is smoothly varying with the load until Point 2 (509 kN). From Fig. 8 (b), it can be seen that the variations of indentation is near zero when the load is varied from zero to Point 1 (290 kN). After that, the indentation starts to increase obviously because of the initiation of yielding in the console (Fig. 9 (a)). When the load of the joint increases to 509 kN, the top part of the webs below the loading area starts to yield (Fig. 9 (b)), which results in the decrease of the vertical stiffness. Correspondingly, the indentation of the top flange increases with the clearly detectable discontinuity of the slope, as shown Point 2 in Fig. 8 (b).

After that, the membrane tension mechanism in the top flange takes a role. Consequently, the forces transferred through the web shear decrease, which stops the increase of the strain L63 between Point 2 and 4 in Fig. 8 (a). Between Point 2 and 4, yield regions develop further. At load value of 643 kN (Point 3), yielding reaches edges of the end plate of the console (Fig. 9 (c)). When the load is further increased to the value of 842 kN, yielding of this endplate reaches the centre (Fig. 9 (d)). Both sudden curling of endplate and sudden involving of bearing area of the top flange of the steel console have been observed (Fig. 9 (d)). After that, the value of the strain of L63 increases again with the load, as shown in Fig. 8 (a). The load transferring from console to column at this stage takes place mainly by both shear and bending of the console webs because the vertical stiffness of the webs takes a role in the joint with the decrease of the membrane tension stiffness of the top flange. This point at which shear and bending of webs start to take a role is defined as limit load of joint (Point 4). The indentation corresponding to Point 4 is about 3.21 mm.

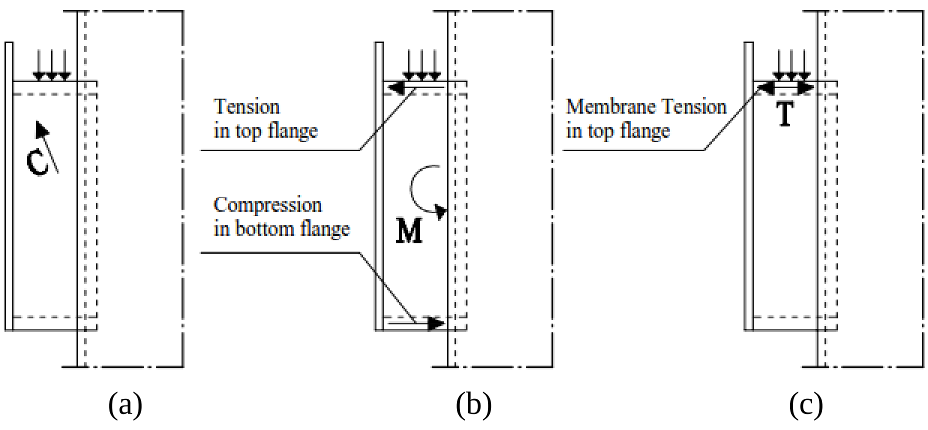

Fig. 7 Three load transferring routes by: (a) shear of web; (b) bending of both web and flanges; (c) membrane tension of top flange developed from indentation.

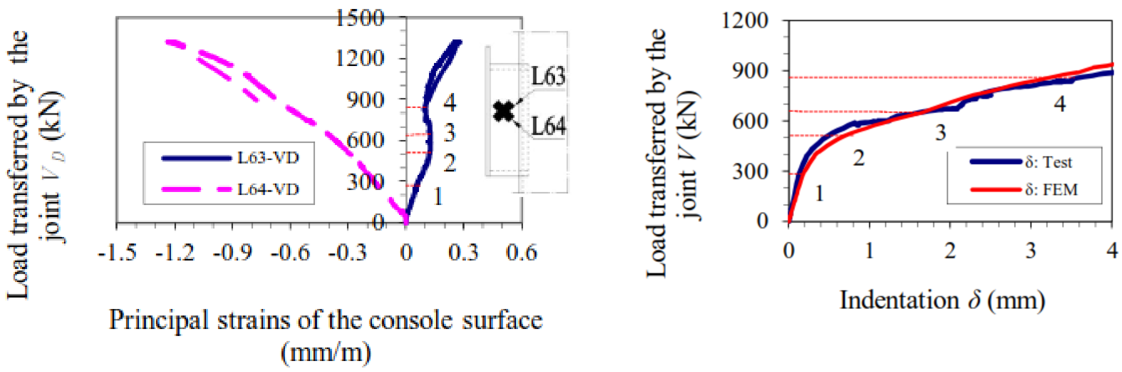

(a) (b)

Fig. 8 Four key points at: (a) Load-tension strain (L63) curve; (b) Load-indentation curve.

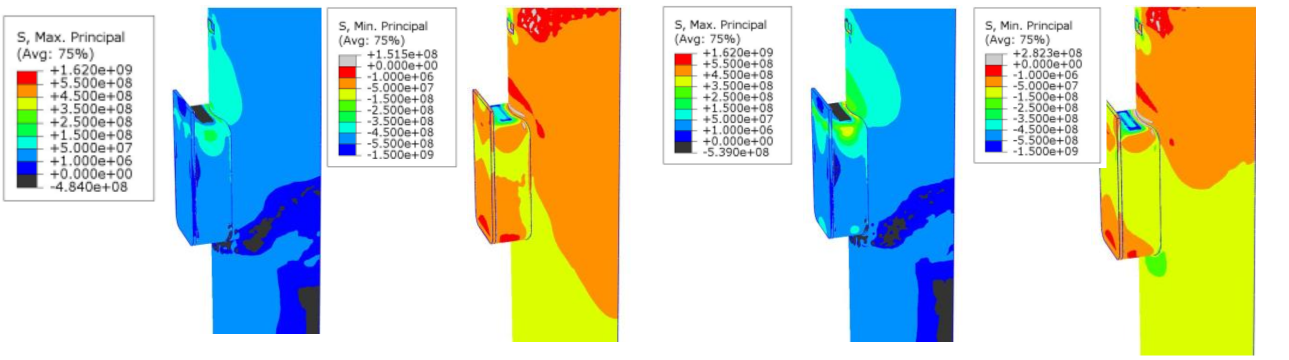

Max Min Max Min

(a) V = 290 kN (b) V = 509 kN

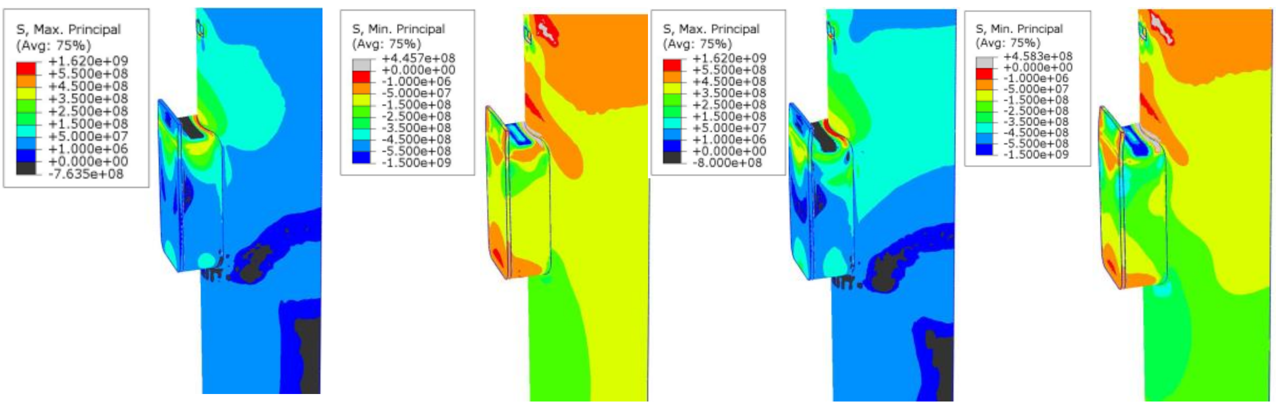

Max Min Max Min

(c) V = 640 kN (d) V = 842 kN

Fig. 9. Maximum and minimum principal stresses at four key points.

5 Parametric Studies

According to the descriptions of the load transferring mechanism, five parameters that could have influence on the behaviour and the limit load of the joint, are investigated. These parameters, as shown in Fig. 10 (a), are:

(1) Flange width of the console (*b* = 100, 150, and 250 mm);

(2) Web height of the console *(h* = 150, 250, and 300 mm);

(3) Section thickness of the console *(t* = 7.1, 8.8, and 10 mm);

(4) Corners of the console (include and exclude);

(5) Gap between the WQ-beam endplate and column face (*d* = 10, 15, and 20 mm).

The load-indentation curves are shown in Fig. 10 (b) to (f) based on the numerical analyses with varying these parameters respectively. The FE analyses are interrupted when the displacements (*S1-S4* as shown in Fig. 3) underneath the WQ-beam along the loading line reach the value of 25 mm. The value of indentation, corresponding to this value is not the same as with the variation of each parameter.

Fig. 10 (b) shows the variation of load-indentation curves with different flange width of the console. The curves are overlapping until initiation of the console yielding, which is approximately 290 kN. After that, the joint carries higher load with the wider flanges as the membrane tension dominating in the top flange until the formation of yielding mechanism. The flange width is a beneficial factor for the limit load of the joint. Since the indentation corresponding to the yielding mechanism will be varied with the variation of flange width, the loads in the joints to start the new shear mechanism will be different. The joint with higher webs exhibits higher load-carrying capacity before the web yielding (Fig. 10 (c)). But the height of the webs has no influence on the formation of yielding mechanisms in the regions close to the top of the console. Therefore, increasing the web height will not increase the limit load of the joint. Increasing the wall thickness of the section is a beneficial factor for both formations of yielding mechanisms close to the top of the console and increasing of compression crushing resistance on the top of the web. Therefore, the joint exhibits higher load with thicker wall thickness at all stages (Fig. 10 (d)). Fig. 10 (e) shows that excluding the round corners in the simulation has only a minor influence on the joint behaviour before the formation of yielding mechanisms. After that, it seems that the rounded corners have small influence on the shearing and the bending of the webs. As shown in Fig. 10 (f), the load capacity of the joint with gap of 10 mm is a little bit higher than the other two cases because of smaller bending arm.

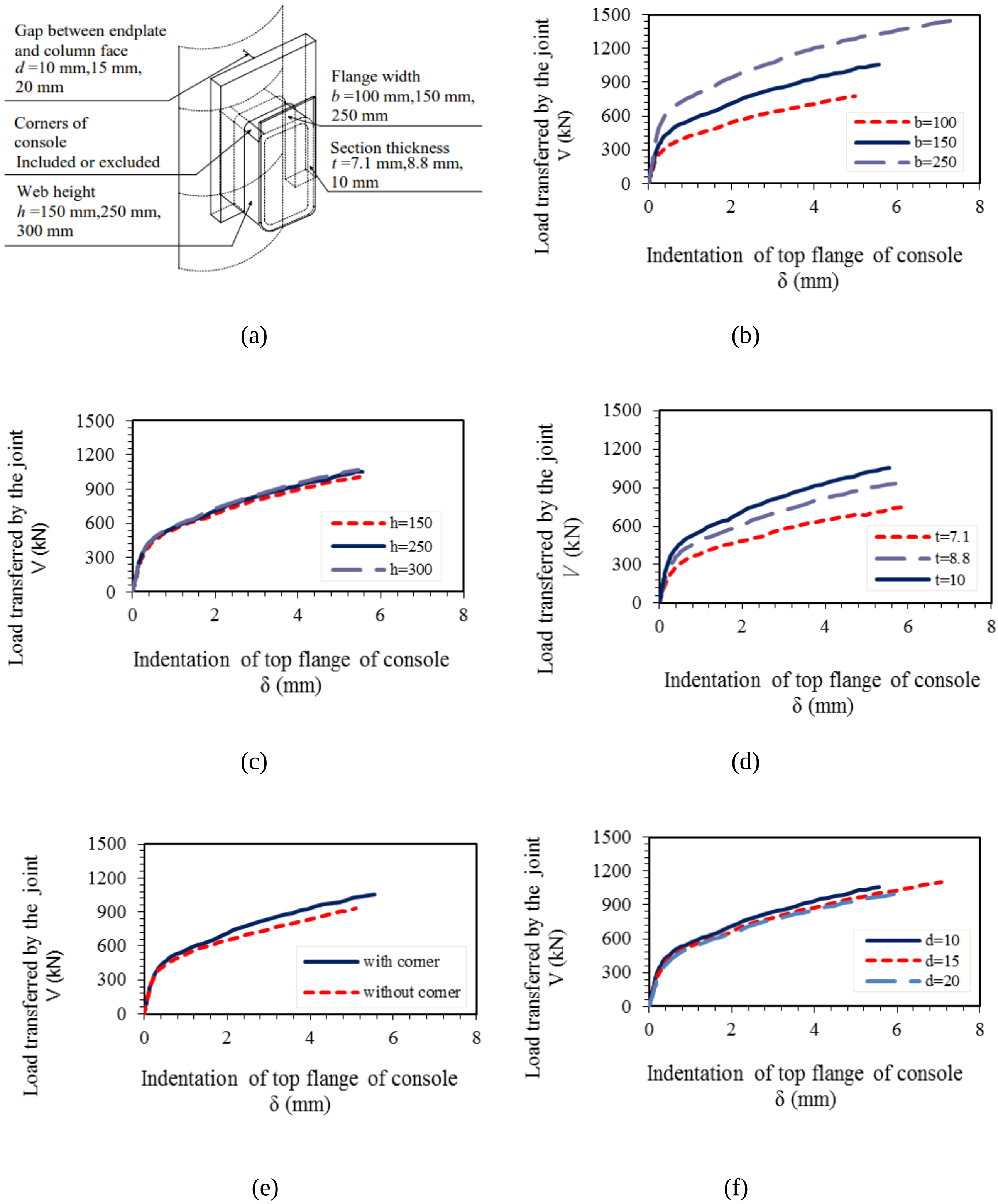

Fig. 10. Load-indentation curves from FE analyses. (a) Definition of parameters; (b) Width of flange; (c) Height of web; (d) Section thickness; (e) Corners of console being included and excluded; (f) Gap between WQ-beam endplate and column face.

6 Proposed criteria to determine yield and ultimate strength of joint

6.1 Criteria for determining both yield and ultimate strength of joint

Determining the ultimate strength of the joint is an important objective in this paper. As mentioned previously, a clear peak load of the joint is not achieved in the tests. Therefore, suitable criteria are required in order to define the yield and the ultimate load of the joint. In this section, the possibilities of applying the available criteria for determining the limit strength of a similar joint found in the literature are discussed first. Then, a new criterion to determine the limit load of the joint is proposed, based on the parametric studies on load transfer mechanism of the joint.

Based on references [12-16], the yield load criterion has been widely used also in the study of tensile behaviour of welded tubular connections. In this criterion, the load-deformation curve is approximated by a bi-linear model. The yield load is defined as the load at the intersection of two lines, the “kink” in the curve where an abrupt change in stiffness occurs, as shown in Fig. 11 (b). The same criterion has been adopted in this paper to determine the yield load of the joint.

The strain-based criterion has been extensively used to define the limit state of structures. Generally, the limit load is assumed to be reached when the equivalent plastic strain achieves the proposed limit value of strain in the numerical analysis. The principal strain value of 5% is proposed by EN 1993-1-5 [17] for the ultimate limit state for the regions subjected to tensile stresses. Besides, the uniform strain of the material with the value of 20% has also been suggested as the strain corresponding to ultimate strength [18-20]. The limiting plastic strain at which cracking starts to take place is not a constant value, it depends on many parameters, for instance, on three-dimensional stress state. However, if the limit strain corresponding to limit state is taken as strain target, and 20% of uniform strain as strain capacity, then the differences between these two strains can be considered as design margin. It seems that the high plastic strain over 20% and up to 40% can also be achieved when the joint is close to the actual failure as shown in Fig. 12 (a) and (b), respectively. The indentations and the limit loads corresponding to these strain limits are shown in Fig. 11 (a). The indentation in the console corresponding to the plastic strain of 40% is up to 14.1 mm, which is too large in practice. Therefore, the loads at plastic strain of both 5% and 20% have been further used to investigate the limit load of the studied joint**.**

The deformation-limit criterion has been used to determine the ultimate strength of tubular joints in which the membrane force in the chord and strain hardening of the material are exhibited [12, 21-24]. Currently, the deformation limit of 3% of the width or diameter chord member adopted by the International Institute of Welding (IIW) [25] is widely accepted as the ultimate deformation limit for a tubular joint with the chord flange failure mode. In addition, the same deformation limit has been applied to determine the ultimate strength of the welded T-joint in cold-formed RHS sections with for the web buckling failure mode [21]. The same limit is adopted to study the limit load of the current joint. The load and the indentation corresponding to 3% of console flange width are shown in Fig. 11(b).

Besides, a new criterion to define the ultimate strength of the joint is proposed based on the failure mechanism of joint. The endplate of WQ-beam is carried by the top flange, which is supported by two webs, endplate of console, and column. When the yielding mechanism is formed among these supporting elements as shown in Fig. 12 (c), it is assumed that the ultimate capacity of the joint has been reached. In addition, the results of parametric studies in Table 2 have shown that the load corresponding to formation of yielding mechanism is close to the load when 10% of the plastic strain is reached. Therefore, similar to the strain-based criterion, the load at plastic strain of 10% is defined as the limit load of the joint as shown in Fig. 11 (b).

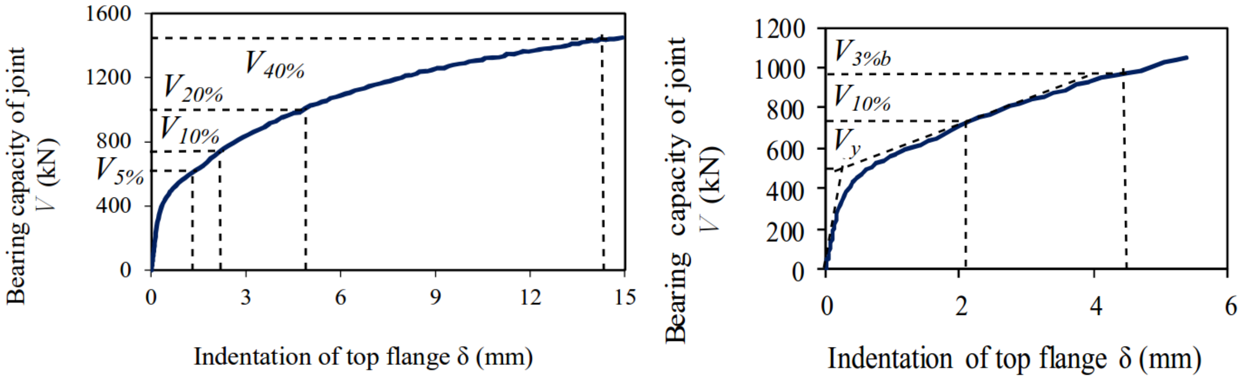

(a) (b)

Fig. 11 Schematic of yield load and ultimate load determination methods from Load–displacement curves: (a) Strain-based criterion; (b) yield load criterion and deformation-based criterion.

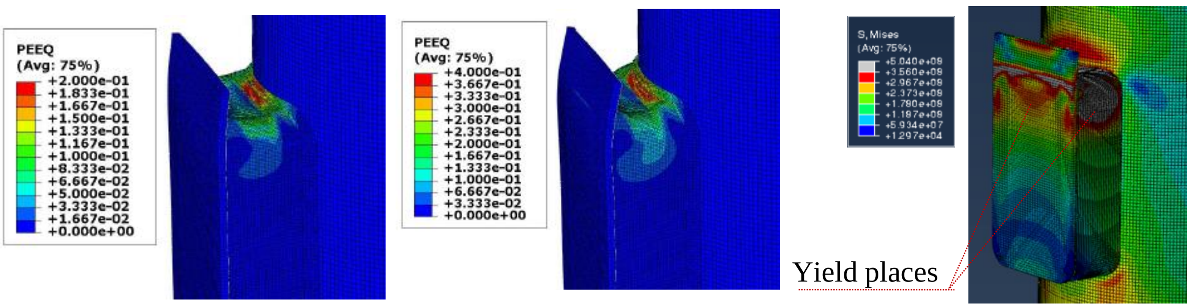

(a) (b) (c)

Fig. 12 Strain and stress distributions at the joint (a) Equivalent plastic strain at PEEQ=0.2; (b) Equivalent plastic strain at PEEQ=0.4; (c) Stress distribution of formation of yielding mechanisms (b=150 mm. h=250 mm, t=10 mm).

6.2 Comparisons and discussions

The proposed limit loads are compared with yield loads, those determined according to strain-based criteria (5% and 20%), and on deformation-based criterion (deformation limit of 3% of flange width of console), respectively. The proposed limit load is also compared with the design resistance of welded joints connecting gusset plate to rectangular tubular chord [9]. Both limit-load values and comparisons results for various joint dimensions are listed in Table 2.

Table 2 shows that the equivalent plastic strains when the yielding mechanism is formed in the joints with various dimensions are approximately 10% with exception of cases of d=15 mm and d=20mm. The maximum plastic strains in these two cases are 4% and 6%, respectively. However, for these two cases, when the equivalent plastic strain in the top flange reaches 10%, the joint still transfers the load with acceptable indentation. Therefore, reaching 10% of equivalent plastic strain is proposed as the criterion to determine the ultimate strength of the joint. The loads and indentations at 10% of plastic strain have been updated in Table 2.

As mentioned before the limit of 20% plastic strain is defined as strain capacity. However, Table 2 shows that for the section of 250 mm x 250 mm x 10 mm, the strain exceeds 20% when 3% of *b* (7.5 mm) is reached. It seems that for these particular dimensions, the 3% of *b* is not a relevant limit. Therefore, further comparisons on limit loads have not included in this particular case. Comparison results in Table 2 show that the proposed limit loads are approximately 21% to 27% smaller than those determined by the criteria of deformation limit and 20% of plastic strain, but 56% to 16% higher than those by the criteria of yield-load and 5% of plastic strain. The values of yield loads are close to those determined at 5% of plastic strain. The load values are all close to the load values when web yielding occurs in the mechanism analyses of load transfer. The joint still has capacity after the web yielding because of the further formation of yielding mechanism. The comparison results also show that the proposed limit loads are closer to the values determined from deformation-based criterion than those from the criterion of 20% of plastic strain. However, it seems that the proposed criteria provide more uniform values of indentation. Therefore, it can be concluded that the proposed criterion is a suitable criterion to determine the limit load of the studied joint.

Since no design rule is provided in current EN 1993-1-8, therefore, the resistance of welded joint when connecting gusset plate to rectangular tubular chord is selected to make comparisons because of the similar joint geometries. The side wall crushing model shown in Fig. 13 [9] is chosen for the comparisons. The equation to determine the design joint resistance is given by the equation (2).

$$N_{1.Rd} = f_{y0} \cdot t_0 \cdot (2t_1 + 10t_0) / \gamma_{M5} \tag{2}$$

where f_{y0} is the yielding stress of the chord, t_1 is the thickness of plate, t_0 is the thickness of the chord, γ_{M5} is partial safety factor. Because the width of the load distributed on the top of the webs is smaller than the value of $2t_1+10t_0$, therefore, the entire length of the webs is used in the calculation to replace $2t_1+10t_0$. In addition, the partial safety factor (γ_{M5}) is taken as 1.0 for the purpose of comparisons,

The studies in [26] have shown that when the limit load is determined by the plastic failure mechanism, both geometrical imperfections and residual stresses have only minor influence on the limit load. FE analyses showed that the yielding of steel console starts from its side wall and the limit state is defined as the yielding reaches the edges of the endplate of steel console. Therefore, the limit loads from FE analyses without imperfections have been compared to those from equation 2 (based on plastic mechanism) to show the contributions of both top flange of steel console and structural redundancy to the joint capacity. However, the sensitivity analyses of FE models to imperfections are necessary if more precise comparisons are carried out. Table 2 shows the joint resistance calculated by equation 2 and the ratio of the yield load and the limit load to the joint strength calculated using sidewall crushing model. The results of comparison show that using sidewall crushing model to estimate the strength of this joints is quite conservative because the contribution of the top flange has not been taken into account as discussed in mechanism analysis of load transfer.

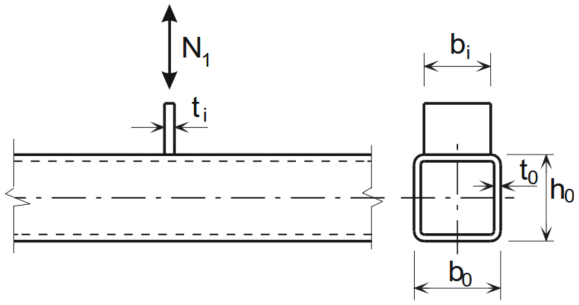

Fig. 13 Side wall crush model provided in EN 1993-1-8 [9].

Table 2 Ultimate strength of joint determined by various criteria for the studied joint dimension

Variations of parameters					Yield load	Proposed criterion			Proposed ultimate strength at 10% of plastic strain			Based on three existing criteria						Comparisons of V_u with V_y, $V_{5\%}$, $V_{20\%}$, and $V_{3\%b}$				Comparisons with sidewall-crush model		
Console				Gap								5% strain		3%*b*		20% strain								
b	h	t	Corner contact	d	V_y	Strain	V_{ua}	δ	V_u	δ	%b	$V_{5\%}$	δ	$V_{3\%b}$	δ	$V_{20\%}$	δ	V_u / V_y	V_u / $V_{5\%}$	V_u / $V_{3\%b}$	V_u / $V_{20\%}$	$N_{1.Rd}$	V_y / $N_{1.Rd}$	V_u / $N_{1.Rd}$
mm	mm	mm		mm	kN	ε	kN	mm	kN	mm		kN	mm	kN	mm	kN	mm					kN		
100	250	10	Yes	10	365	0.09	533	1.91	548	2.03	2.03	469	1.43	633	3.0	778	5.0	1.50	1.17	0.87	0.70	426	0.86	1.29
150	250	10	Yes	10	509	0.10	772	2.43	772	2.43	1.62	649	1.65	965	4.5	1050	5.5	1.52	1.19	0.80	0.74	454	1.12	1.70
250	250	10	Yes	10	698	0.09	1066	2.90	1095	3.12	1.25	896	1.72	1458	7.5	1320	5.4	1.57	1.22	-	0.83	462	1.51	2.37
150	**150**	10	Yes	10	497	0.10	763	2.58	767	2.62	1.75	617	1.50	940	4.5	1006	5.5	1.54	1.24	0.82	0.76	454	1.09	1.69
150	**250**	10	Yes	10	509	0.10	772	2.43	772	2.43	1.62	649	1.65	965	4.5	1050	5.5	1.52	1.19	0.80	0.74	454	1.12	1.70
150	**300**	10	Yes	10	514	0.10	775	2.34	775	2.34	1.56	659	1.58	995	4.5	1072	5.5	1.51	1.18	0.78	0.72	454	1.13	1.71
150	250	**7.1**	Yes	10	332	0.10	551	2.73	582	3.03	2.02	462	1.72	680	4.5	745	5.8	1.75	1.26	0.86	0.78	323	1.03	1.80
150	250	**8.8**	Yes	10	418	0.10	695	2.68	695	2.68	1.79	575	1.71	857	4.5	935	5.7	1.66	1.21	0.81	0.74	400	1.05	1.74
150	250	**10**	Yes	10	509	0.10	772	2.43	772	2.43	1.62	649	1.65	965	4.5	1050	5.5	1.52	1.19	0.80	0.74	454	1.12	1.70
150	250	10	Yes	**10**	509	0.10	772	2.43	772	2.43	1.62	649	1.65	965	4.5	1050	5.5	1.52	1.19	0.80	0.74	454	1.12	1.70
150	250	10	Yes	**15**	511	0.04	711	2.29	859	3.78	2.52	729	2.44	923	4.5	1100	7.3	1.68	1.18	0.93	0.78	454	1.13	1.89
150	250	10	Yes	**20**	508	0.06	702	2.38	802	3.35	2.23	662	2.10	893	4.5	992	5.9	1.58	1.21	0.90	0.81	454	1.12	1.77
150	250	10	**No**	10	510	0.08	692	2.41	763	3.15	2.10	610	1.62	883	4.5	931	5.1	1.50	1.25	0.86	0.82	454	1.12	1.68
150	250	10	**Yes**	10	509	0.10	772	2.43	772	2.43	1.62	649	1.65	965	4.5	1050	5.5	1.52	1.19	0.80	0.74	454	1.12	1.70

7 Conclusions

A 3D finite element model considering both material and geometrical non-linearity is created to simulate a novel, double-sided, composite beam-to-column joint in a slim floor frame system. The comparisons between the load-deformation behaviour of the joint in tests and numerical results are in good agreement. This proves that the FE model presented is capable of predicting the response of the joint to an acceptable degree of accuracy and can be used in further studies. The load-transfer mechanism studies performed show that about 94% of the load on the beam is transferred to the column through the steel console. The load is transferred through both the tension developed in the top flange and shear in the webs. The tension of the top flange is from both the bending of the cross-section and the yielding mechanism after the web yielding. Further parametric analyses indicate that the flange width, the section thickness, and the contact between the corners and WQ-beam endplate have positive effects on the strength of the joint. This is due to the tension developed in the top flange. The web height has only a minor influence on the strength of the joint because of the bearing yielding of the webs. The gap between the WQ-beam endplate and column face has insignificant influence on the strength of the joint. Since no obvious yield or peak load can be directly determined on the base of load-deflection curves, the load at equivalent plastic strain of 10% is proposed to be the limit load of the joint, based on the results from parametric analyses. The load determined by the proposed criterion is closed to that when the yielding mechanism is formed inside the joint. Comparison between the values of the proposed limit load and those determined on the base of different other criteria shows that the proposed criteria provide good estimation of joint resistance with reasonable indentations.

Acknowledgement

The authors would like to acknowledge the main financial support provided for this work by Ruukki Construction Oy and Academy of Finland. In addition, the financial support from Pöyry Finland Oy is highly appreciated. The authors would like to thank also Emeritus Professor Pentti Mäkeläinen for initiation this research project. Warm thanks for the technical help in using the ABAQUS code, is directed to Mr. Reijo Lindgren, the specialist of IT Centre for Science Ltd (CSC).

References

[1] Z.C. Ma, P. Mäkeläinen, Structural behaviour of composite slim floor frames in fire conditions, J. Construct. Steel Res. 62 (2006) 1282-1289.

[2] M. Malaska, Behaviour of a semi-continuous beam-column connection for composite slim floor, Ph.D thesis, Aalto university, Helsinki, 2000.

[3] J.K. Ahn, C.H. Lee, Fire behavior and resistance of partially encased and slim-floor composite beams, J Construct. Steel Res. 129 (2017) 276–285.

[4] L. Toi, S.M. Chen, Numerical procedure for nonlinear behavior analysis of composite slim floor beam, J Construct. Steel Res. 106 (2015) 209–219.

[5] D. Lam, X.H. Dai, U. Kuhlmann, J. Raichle, M. Braun, Slim-floor construction-design for ultimate limit state, Steel Construction 8 (2) (2015) 79–84.

[6] G. Hauf, U. Kuhlmann, Deformation calculation methods for slim floors, Steel Construction 8 (2) (2015) 96–101.

[7] E. Hömmö, Design methods for console joint of the composite column and WQ-beam, Master thesis, Tampere university of technology, Tampere, 2009.

[8] Eurocode 4, Part 1-1: Design of composite steel and concrete structures: General rules and rules for buildings. EN 1994-1-1: December 2004.

[9] Eurocode 3, Part 1-8: Design of steel structures: Design of joints. EN 1993-1-8: May 2005.

[10] ABAQUS, User's Manual, version6.13, Hibbitt, Karlsson & Sorensen Inc., 2013.

[11] Eurocode 2, Part 1-1: Design of concrete structures: General rules and rules for buildings. EN 1992-1-1, April, 2004.

[12] N. Kosteski, J.A. Packer, R.S. Puthli, A finite element method based yield load determination procedure for hollow structural section connections, J Construct. Steel Res. 59 (2003) 453-471.

[13] X.L. Zhao, G.J. Hancock, T-joints in rectangular hollow sections subject to combined actions, J Struct. Engng. 117 (8) (1991) 2258–2277.

[14] J.A. Packer, G. Davies, M.G. Coutie, Yield strength of gapped joints in rectangular hollow section trusses. Proceedings—Institution of Civil Engineers, Part 2 1980;69:995–1013.

[15] Y. Kurobane, Y. Makino, K. Ochi, Ultimate resistance of unstiffened tubular joints, J Struct. Engng. 110 (2) (1984) 385–400.

[16] T. Kamba, C. Taclendo, CHS column connections without stiffeners, Proc. Eighth International Symposium on Tubular Structures, Singapore, 1998:567–76.

[17] Eurocode 3, Part 1-5. Design of steel structures: Plated structural elements. EN 1993-1-5: October 2006.

[18] EN 10219-1, Part 1: Cold formed welded structural hollow sections of non-alloy and fine grain steels: Technical delivery conditions. March 2006.

[19] EN 10025-2, Part 2: Hot rolled products of structural steels: Technical delivery conditions for non-alloy structural steels. November 2004.

[20] H. Raiko, Design analysis report for the canister, Technical report, TR-10-28. VTT, Helsinki, April 2010.

[21] X.L. Zhao, Deformation limit and ultimate strength of welded T-joints in cold-formed RHS sections, J Construct. Steel Res. 53 (2000) 149-165.

[22] L.H. Lu, G.D. de Winkel, Y. Yu, J. Wardenier, In: Deformation limit for the ultimate strength of hollow section joints. Tubular structures VI, Rotterdam: Balkema, 1994:341–347.

[23] R.M. Korol, F.A. Mirza, Finite element analysis of RHS T-joints, J Struct. Engng. 108 (9) (1982) 2081–2098.

[24] J. Mouty, In: Theoretical prediction of welded joint strength, Proceedings of the International Symposium on Hollow Structural Sections, Toronto (Canada), 1977.

[25] International Institute of Welding (IIW). Design recommendations for hollow section joints – predominantly statically loaded. IIW Doc. XV-701-89, 2nd ed, IIW Subcommission XV-E, Helsinki, 1989.

[26] P. Granath, Behavior of slender plate girders subjected to patch loading, J. Construct. Steel Res. 42 (1997) 1-19.